Materials Science in Semiconductor Processing 18 (2014) 160–164

Contents lists available at ScienceDirect

Materials Science in Semiconductor Processing

journal homepage: www.elsevier.com/locate/mssp

Enhanced formaldehyde-sensing properties of mixed Fe_2O_3–In_2O_3 nanotubes

Xiao Chi [a], Changbai Liu [b], Li Liu [a,*], Shouchun Li [a], Haiying Li [a], Xiaobo Zhang [a], Xiaoqing Bo [a], Hao Shan [a]

[a] State Key Laboratory of Superhard Materials, College of Physics, Jilin University, Changchun 130012, PR China
[b] College of Electronic Science & Engineering, Jilin University, Changchun 130012, PR China

ARTICLE INFO

Article history:
Received 14 July 2013
Received in revised form
9 October 2013
Accepted 11 November 2013
Available online 10 December 2013

Keywords:
In_2O_3
Fe_2O_3
Nanotubes
Gas sensor
Formaldehyde

ABSTRACT

Pure In_2O_3 and mixed Fe_2O_3–In_2O_3 nanotubes were prepared by simple electrospinning and subsequent calcination. The as-prepared nanotubes were characterized by scanning electron microscopy, powder X-ray diffraction, and energy-dispersive X-ray spectrometry. Gas sensors were fabricated to investigate the gas-sensing properties of In_2O_3 and Fe_2O_3–In_2O_3 nanotubes. Compared to pure In_2O_3, Fe_2O_3–In_2O_3 nanotubes exhibited better gas-sensing properties for formaldehyde at 250 °C. The response of the Fe_2O_3–In_2O_3 nanotube gas sensor to 100 ppm formaldehyde was approximately 33, which is approximately double the response of the pure In_2O_3 nanotube gas sensor. In both cases the response time was ~5 s and the recovery time was ~25 s.

© 2013 Elsevier Ltd. All rights reserved.

1. Introduction

Many studies have investigated metal-oxide nanostructures. Compared to the bulk structures, metal-oxide nanostructures usually have better properties and are suitable for applications such as solar cells [1], electrode materials [2], catalysts [3], humidity sensors [4], and gas sensors [5]. Gas sensors have been investigated for the detection of many different gases, including ethanol, ammonia, acetone, H_2S, O_3, NO_2, and H_2 [6–12]. Gas sensors with outstanding gas-sensing properties usually have an open-edge geometry [13]. Hollow, porous, and hierarchical nanostructures are effective [14–16]. Nevertheless, some sensing materials with a good nanostructure exhibit mediocre gas-sensing properties [17]. It is widely accepted that mixing or doping is a convenient and efficient way to improve sensor performance [18–20].

As a volatile organic pollutant in indoor environments, formaldehyde vapor is harmful to human health. It can lead to cancer, pulmonary damage, and leukemia [21]. In_2O_3 and Fe_2O_3 are both n-type semiconductors with gas-sensing properties for formaldehyde [21,22]. However, their formaldehyde-sensing properties are not outstanding and they suffer from shortcomings such as low sensitivity, slow response and recovery, and a narrow detection range.

We synthesized Fe_2O_3–In_2O_3 nanotubes by electrospinning and subsequent calcination. Gas sensors were fabricated to investigate the formaldehyde gas-sensing properties of Fe_2O_3–In_2O_3 and pure In_2O_3 nanotubes. The results reveal that Fe_2O_3–In_2O_3 nanotube sensors have a better response than In_2O_3 nanotube sensors.

2. Experimental

2.1. Materials

Indium nitrate hydrate ($In(NO_3)_3$, 99.99%), ferric nitrate ($Fe(NO_3)_3 \cdot 9H_2O$, 99.99%), *N*,*N*-dimethylformamide (DMF,

* Corresponding author. Tel./fax: +86 431 8502260.
E-mail address: liul99@jlu.edu.cn (L. Liu).

1369-8001/$ - see front matter © 2013 Elsevier Ltd. All rights reserved.
http://dx.doi.org/10.1016/j.mssp.2013.11.016

≥99.9%), and ethanol (≥99.5%) were purchased from Aladdin (China). Poly(vinyl pyrrolidone) (PVP; M_w= 1,300,000) was purchased from Sigma-Aldrich (USA).

2.2. Sample preparation

In_2O_3 and Fe_2O_3–In_2O_3 nanotubes were synthesized as follows. $In(NO_3)_3$ (0.8 g) and $Fe(NO_3)_3 \cdot 9H_2O$ (0.096 g) were mixed with 8 g of DMF and 8 g of ethanol under magnetic stirring for 30 min. In a separate container, 1.2 g of PVP was mixed with 8 g of ethanol under vigorous stirring for 30 min. The two solutions were then mixed and stirred vigorously for 10 h to obtain the precursor solution. The process for pure In_2O_3 nanotubes was the same but without $Fe(NO_3)_3 \cdot 9H_2O$. The precursor was injected using a syringe. The distance between the syringe (anode) and the collector (cathode) was 20 cm and the voltage was 15 kV. Then composite fibers in the form of non-woven mats were collected and calcinated at 550 °C for 2 h at the heating rate of 5 °C/min.

Gas sensors were fabricated as follows. The as-prepared nanotubes were mixed with deionized water at a ratio of 100:25 (w/w) to form a paste. The paste was coated onto a ceramic tube on which a pair of Au electrodes was previously printed. A Ni–Cr heating resistance wire was inserted into the ceramic tube to provide the working temperature. The devices were aged for more than 3 days. On the first day, the sensors were stored at room temperature until the paste on the ceramic tube was dry. On the second day, the sensors were aged on a stage at 300 °C for 24 h. On the third day, sensors were stored at room temperature until the sensing properties were tested.

2.3. Measurement

Gas-sensing tests were conducted using a modified CGS-8 gas-sensing analysis system (Beijing Elite Tech Co., China). The response of sensors was studied in a sealed test chamber. The target gas was diluted with air. Before testing was started, the gas sensors were stabilized at the desired temperature. When the sensor resistance was stable, the target gas was injected into the test chamber via a micro-injector through a rubber plug. After the resistance reached a new value, the test chamber was opened for gas sensor recovery in air. The sensor resistance and response values were recorded by the analysis system.

The sensor response was defined as R_a/R_g, where R_a is the resistance in ambient air and R_g is the resistance in the target gas. The response and recovery times were defined as the time taken by the sensor to reach 90% of the total resistance change for adsorption and desorption, respectively [23].

Powder X-ray diffraction (XRD) analysis was conducted on PANalytical Empyrean diffractometer with Cu K_α radiation (λ=1.5406 Å). Scanning electron microscope (SEM) images were recorded using an FEL XL30ESEM instrument. Energy-dispersive X-ray (EDX) spectrometry was performed using an FEL XL30ESEM-FEG system.

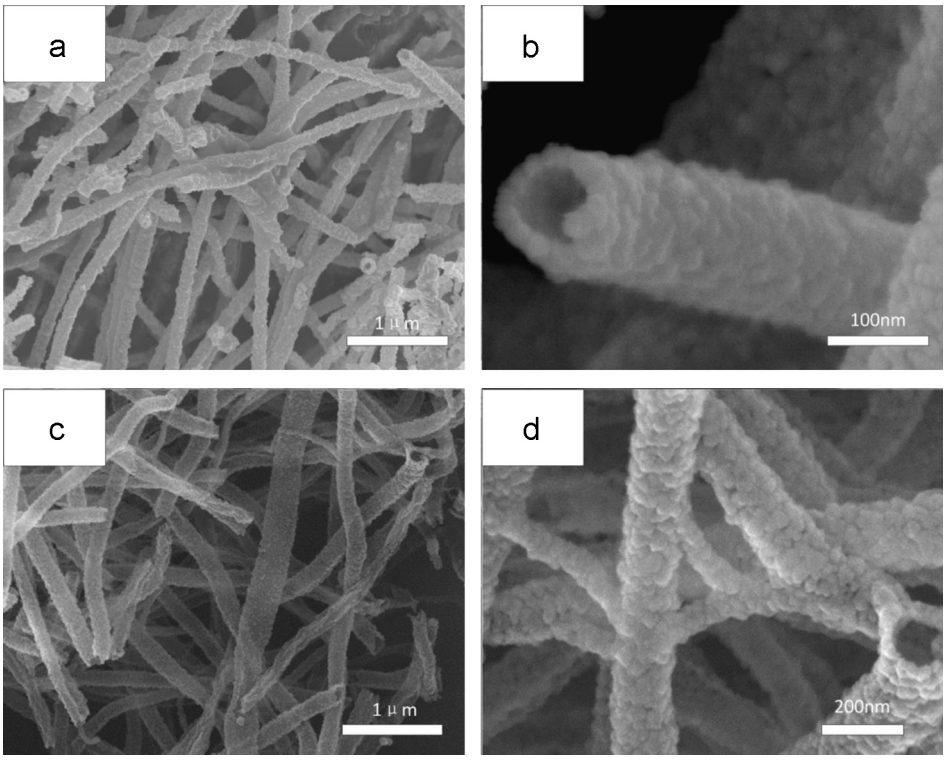

Fig. 1. SEM images of (a,b) In_2O_3 and (c,d) Fe_2O_3–In_2O_3 nanotubes after annealing at 500 °C.

3. Results and discussion

3.1. Morphological and structural characteristics

Fig. 1 shows SEM images of In_2O_3 and Fe_2O_3–In_2O_3 nanotubes annealed at 550 °C. The SEM images of high magnification images are presented in Figs. 1(b) and (d), respectively. We can see that the diameter of nanotubes is substantially uniform, which is about 200 nm. The morphology of nanotubes is obvious in each image of Fig. 1. These nanotubes can provide more space for gas molecules penetrating into the materials for gas sensing response and recovery.

XRD patterns for In_2O_3 and Fe_2O_3–In_2O_3 nanotubes are shown in Fig. 2. The primary peaks can be indexed to cubic single-crystal In_2O_3. The parameters agree well with JCPDS card 71–2195, without any impurity peaks, confirming that all the nanotubes were of high purity. The lattice constants are $a=c=10.117$ Å according to the Debye–Scherrer formula

$$D = K\lambda/\beta \cos(\theta),$$

where D is the crystallite size, K is a constant (0.89), λ is the X-ray wavelength (0.15406 nm), and β is the full width at half-maximum of the 2θ diffraction peak [21,24]. The average crystallite size was 20.7 nm for In_2O_3 and 13.3 nm for Fe_2O_3–In_2O_3 nanotubes. The XRD peaks are sharper and narrower for In_2O_3 than for Fe_2O_3–In_2O_3 nanotubes. According to the Debye–Scherrer formula, a narrower peak leads to a greater grain size. This can be ascribed to the larger radius of In^{3+}, which has five layers of electrons, compared to four layers for Fe^{3+}. Therefore, the radius of In_2O_3 is larger than that of Fe_2O_3. The small amount of In^{3+} replaced by Fe^{3+} causes a decrease in the average unit cell size. The bond strength and binding energy also affect the average particle size [25]. For all these reasons, the average grain size is smaller for Fe_2O_3–In_2O_3 than for In_2O_3.

EDX data for Fe_2O_3–In_2O_3 nanotubes (Fig. 3) reveal the presence of Fe, which cannot be observed in Fig. 2b. This suggests that Fe_2O_3–In_2O_3 nanotubes were successfully synthesized by electrospinning. The samples were capped with Pt before EDX analysis and there is evidence of Pt in Fig. 3. The C detected may come from the substrate and incomplete combustion of PVP.

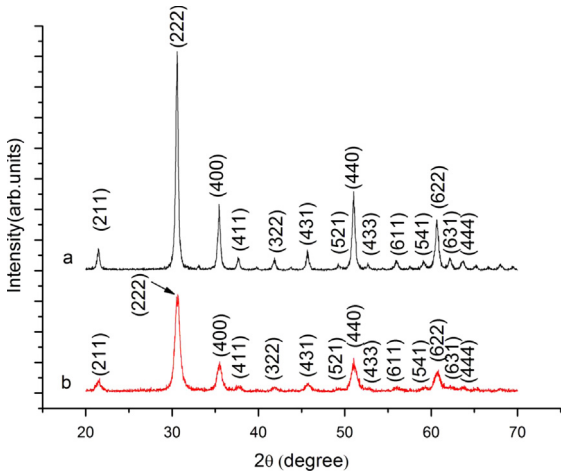

Fig. 2. XRD patterns for (a) In_2O_3 and (b) Fe_2O_3–In_2O_3 nanotubes.

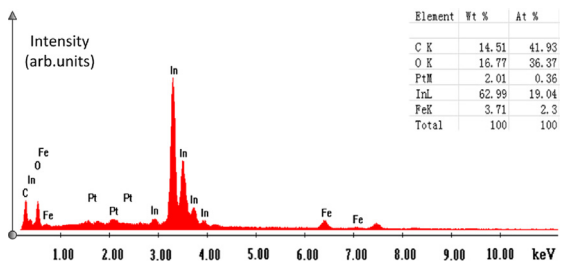

Fig. 3. EDX patterns for Fe_2O_3–In_2O_3 nanotubes.

3.2. Gas-sensing properties

Gas-sensing experiments were performed at different temperatures to find the optimum temperature for formaldehyde detection. Fig. 4 shows the relationship between sensor response to 100 ppm formaldehyde and operating temperature. The response increases with temperature and

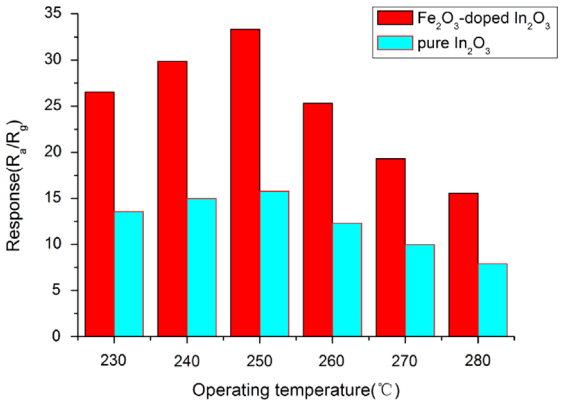

Fig. 4. Response of In_2O_3 and Fe_2O_3–In_2O_3 nanotubes to 100 ppm formaldehyde at different operating temperatures.

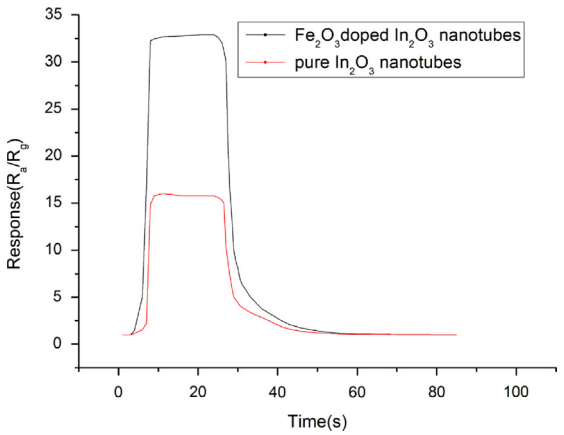

Fig. 5. Response and recovery curves for In_2O_3 and Fe_2O_3–In_2O_3 nanotube gas sensors to 100 ppm formaldehyde.

reaches a maximum at 250 °C, and then quickly decreases with further increases in temperature. The response was 15.78 for the In_2O_3 nanotube sensor and 33.33 for the Fe_2O_3–In_2O_3 nanotube sensor, which is more than double the response of the In_2O_3 sensor. We chose 250 °C as the working temperature for further experiments.

Response and recovery times are important for practical application of gas sensors. Fig. 5 shows the response over time for In_2O_3 and Fe_2O_3–In_2O_3 nanotubes to 100 ppm formaldehyde. The results show that both sensors had fast response and recovery times. In both cases the response time was ~5 s and the recovery time was ~25 s.

To further investigate the response, Fe_2O_3–In_2O_3 nanotube sensors were exposed to different formaldehyde concentrations at 250 °C. The gas sensor response increased linearly from 1 to 100 ppm and then increased more slowly and reached a plateau at 9000 ppm (Fig. 6). The results reveal that the Fe_2O_3–In_2O_3 nanotube gas sensor can detect formaldehyde down to 1 ppm with a response of 2.12, which is very important for high-sensitivity applications.

The sensing properties of Fe_2O_3–In_2O_3 nanotubes for formaldehyde are comparable to those of sensors based on γ-Fe_2O_3 nanofilms (5.5–100 ppm) [22], thick NiO nanofilms (2.1–5 ppm) [26], and Ce-doped SnO_2 nanomaterial (15–100 ppm) [27]. Our gas sensor has a higher response than TiO_2 nanotubes (response time 180 s, recovery 780 s) [28] and ZnO micro-octahedrons (response time < 46 s, working temperature 400 °C) [29]. The response and recovery times in our work were approximately 5 s and 25 s, respectively, and the working temperature was 250 °C. Fe_2O_3–In_2O_3 nanotubes sensors had fast response and recovery times, a low working temperature, a low detection limit, and a high response. Thus, our Fe_2O_3–In_2O_3 nanotube gas sensor has comprehensive properties for gas sensing.

3.3. Gas-sensing mechanism

The change in resistance for a metal oxide sensor can be ascribed to adsorption and desorption of gas molecules that react on the sensor surface. The gas-sensing mechanism can be explained as follows. Gas detection by resistance-type gas sensors depends on the concentration and temperature of the target gas. When a gas sensor is exposed in air, O_2 can chemisorb onto the surface of the gas-sensing material and react with electrons in the conduction band according to [21]

$$O_{2(air)} + 2e^-_{(cond.band)} \rightarrow 2O^-_{(ads.)}. \quad (1)$$

when gas-sensing material is exposed to formaldehyde at 250 °C, formaldehyde molecules can react with adsorbed oxygen species on the surface and release electrons in the conduction band, leading to a decrease in resistance. The reaction is [21]

$$HCHO + 2O^-_{(ads.)} \rightarrow H_2O + CO_2 + e^-. \quad (2)$$

The performance of Fe_2O_3–In_2O_3 nanotubes is better than that of pure In_2O_3 nanotubes. This can be attributed to the formation of a heterojunction between Fe_2O_3 and In_2O_3. Fe_2O_3–In_2O_3 has a lower bandgap than that of pure In_2O_3. Electrons flow to In_2O_3 from Fe_2O_3 and accumulate on the surface of the heterojunction. When exposed to formaldehyde, the heterojunction can adsorb many more formaldehyde molecules than pure In_2O_3 can, which is responsible for the better sensitivity of the Fe_2O_3–In_2O_3 nanotube sensors [30,31].

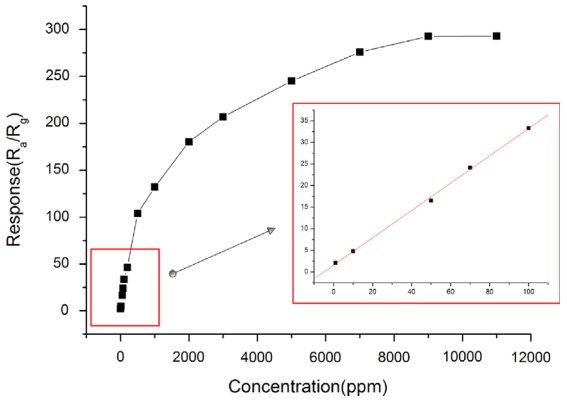

Fig. 6. Response of Fe_2O_3–In_2O_3 nanotube sensors to different formaldehyde concentrations at 250 °C. The inset shows the calibration curve for 1–100 ppm.

4. Conclusion

In_2O_3 and Fe_2O_3–In_2O_3 nanotubes were prepared by electrospinning and subsequent calcination. Experiments revealed that Fe_2O_3 addition can enhance the formaldehyde-sensing properties of In_2O_3 nanotubes. The response of Fe_2O_3–In_2O_3 nanotube gas sensors to 100 ppm formaldehyde was approximately double that of In_2O_3 nanotubes. The response and recovery times were 5 s and 25 s, respectively. The results indicate that Fe_2O_3–In_2O_3 nanotube gas sensors may be good candidates for practical application in formaldehyde sensors.

Acknowledgments

This work was supported by the Jilin Environment Office (2009-22), the Jilin Provincial Science and Technology Department (20100344), and the National Innovation Experiment Program for University Students (2010C65188).

References

[1] A. Subramanian, C.-Y. Ho, H. Wang, J. Alloys Compd. 572 (2013) 11–16.
[2] T. Minami, Semicond. Sci. Technol. 20 (2005) S35–S44.
[3] Y.J. Zhang, L.C. Liu, L.L. Ni, B.L. Wang, Appl. Catal. B 138–139 (2013) 9–16.
[4] J. Zhao, Y. Liu, X. Li, G. Lu, L. You, X. Liang, F. Liu, T. Zhang, Y. Du, Sensors Actuators B 181 (2013) 802–809.
[5] S. Park, H. Ko, S. An, W.I. Lee, S. Lee, C. Lee, Ceram. Int. 39 (2013) 5255–5262.
[6] S.-J. Kim, I.-S. Hwang, J.-K. Choi, Y.C. Kang, J.-H. Lee, Sensors Actuators B 155 (2011) 512–518.
[7] J.-Y. Leng, X.-J. Xu, N. Lv, H.-T. Fan, T. Zhang, J. Colloid Interface Sci. 356 (2011) 54–57.
[8] S. Wei, M. Zhou, W. Du, Sensors Actuators B 160 (2011) 753–759.

[9] M. Zhao, X. Wang, L. Ning, J. Jia, X. Li, L. Cao, Sensors Actuators B 156 (2011) 588–592.
[10] G. Korotcenkov, B.K. Cho, I. Boris, S.H. Han, Y. Lychkovsky, G. Karkotsky, Sensors Actuators B 174 (2012) 586–593.
[11] C. Chen, Y. Wei, G. Sun, B. Shao, Chem. Asian J. 7 (2012) 1018–1025.
[12] Y. Liu, C. Gao, X. Pan, X. An, Y. Xie, M. Zhou, J. Song, H. Zhang, Z. Liu, Q. Zhao, Y. Zhang, E. Xie, Appl. Surf. Sci. 257 (2011) 2264–2268.
[13] S. An, S. Park, H. Ko, C. Jin, W.I. Lee, C. Lee, J. Phys. Chem. Solids 74 (2013) 979–984.
[14] X. Zhao, M. Cao, C. Hu, Mater. Res. Bull. 48 (2013) 2289–2295.
[15] W. Guo, T. Liu, J. Wang, W. Yu, R. Sun, Y. Chen, S. Hussain, X. Peng, Z. Wang, Ceram. Int. 39 (2013) 5919–5924.
[16] P. Sun, Y. Cai, S. Du, X. Xu, L. You, J. Ma, F. Liu, X. Liang, Y. Sun, G. Lu, Sensors Actuators B 182 (2013) 336–343.
[17] P. Song, Q. Wang, Z. Yang, Mater. Lett. 86 (2012) 168–170.
[18] G. Korotcenkov, I. Boris, V. Brinzari, S.H. Han, B.K. Cho, Sensors Actuators B 182 (2013) 112–124.
[19] M. Hu, W.-D. Wang, P. Zeng, J. Zeng, Y.-X. Qin, Chin. Phys. B 21 (2012) 023101.
[20] C.-H. Lin, W.-C. Chang, X. Qi, Procedia Eng 36 (2012) 476–481.
[21] P. Song, Q. Wang, Z. Yang, Sensors Actuators B 168 (2012) 421–428.
[22] K. Huang, L. Kong, F. Yuan, C. Xie, Appl. Surf. Sci. 270 (2013) 405–410.
[23] L. Liu, Y. Zhang, G. Wang, S. Li, L. Wang, Y. Han, X. Jiang, A. Wei, Sensors Actuators B 160 (2011) 448–454.
[24] H. Shan, C. Liu, L. Liu, S. Li, L. Wang, X. Zhang, X. Bo, X. Chi, Sensors Actuators B 184 (2013) 243–247.
[25] M.A. Gabal, A.M. Abdel-Daiem, Y.M. Al Angari, I.M. Ismail, Polyhedron 57 (2013) 105–111.
[26] I. Castro-Hurtado, C. Malagù, S. Morandi, N. Pérez, G.G. Mandayo, E. Castaño, Acta Mater. 61 (2013) 1146–1153.
[27] D. Liu, T. Liu, H. Zhang, C. Lv, W. Zeng, J. Zhang, Mater. Sci. Semicond. Process 15 (2012) 438–444.
[28] G. Wu, J. Zhang, X. Wang, J. Liao, H. Xia, S.A. Akbar, J. Li, S. Lin, X. Li, J. Wang, Ceram. Int. 38 (2012) 6341–6347.
[29] L. Zhang, J. Zhao, H. Lu, L. Gong, L. Li, J. Zheng, H. Li, Z. Zhu, Sensors Actuators B 160 (2011) 364–370.
[30] P. Li, H. Fan, Y. Cai, Sensors Actuators B 185 (2013) 110–116.
[31] M. Ivanovskaya, D. Kotsikau, G. Faglia, P. Nelli, S. Irkaev, Sensors Actuators B 93 (2003) 422–430.